Critical review of Quark Gluon Plasma Signatures

Jens Berger[*], Ulrich Eichmann[†], Sevil Salur[**], Stefan Scherer[†], Detlef Zschiesche[†] and Horst Stöcker[†]

[*]*Institut für Kernphysik, Johann Wolfgang Goethe-Universität, D-60486 Frankfurt am Main, Germany*
[†]*Institut für Theoretische Physik, Johann Wolfgang Goethe-Universität, D-60054 Frankfurt am Main, Germany*
[**]*A.W. Wright Nuclear Structure Laboratory, Yale University, New Haven, CT*

Abstract. We discuss the uniqueness of often proposed experimental signatures for quark matter formation in relativistic heavy ion collisions, using insight gained from non-equilibrium models (three-fluid hydrodynamics and the hadronic transport model UrQMD).

It is demonstrated that these two models – although they do treat the most interesting early phase of the collisions quite differently (thermalizing QGP vs. coherent color fields with virtual particles) – both yield a reasonable agreement with a large variety of the available heavy ion data.

Hadron/hyperon yields, including J/Ψ meson production/suppression, strange matter formation, dileptons, and directed flow (bounce-off and squeeze-out) are investigated. Observations of interesting phenomena in dense matter are reported.

However, we emphasize the need for systematic future measurements to search for simultaneous irregularities in the excitation functions of several observables in order to come close to pinning the properties of hot, dense QCD matter from data.

INTRODUCTION

In the last few years researchers at Brookhaven and CERN have succeeded to measure a wide spectrum of observables with heavy ion beams, $Au+Au$ and $Pb+Pb$. While these programs continue to measure with greater precision the beam energy-, nuclear size-, and centrality dependence of those observables, it is important to recognize the major milestones passed thus far in that work. The experiments have conclusively demonstrated

- stopping and directed collective transverse and longitudinal flow of baryons and mesons – in and out of the impact plane, both at AGS and SPS energies –,
- hadronic resonance production,
- strangeness enhancement,
- the existence of strong nuclear A dependence of, among others, J/ψ and ψ' meson production and suppression.
- dilepton-enhancement below and above the ρ meson mass, and

These observations support that a novel form of "resonance matter" at high energy- and baryon density has been created in nuclear collisions. The global multiplicity and

transverse energy measurements prove that substantially more entropy is produced in $A+A$ collisions at the SPS than simple superposition of $A \times pp$ would imply. Multiple initial and final state interactions play a critical role in all observables. The high mid-rapidity baryon density (stopping) and the observed collective transverse and directed flow patterns constitute one of the strongest evidence for the existence of an extended period ($\Delta\tau \approx 10$ fm/c) of high pressure and strong final state interactions. The enhanced ψ' suppression in $S+U$ relative to $p+A$ also attests to this fact. The anomalous low mass dilepton enhancement shows that substantial in-medium modifications of multiple collision dynamics exists, probably related to in-medium collisional broadening of vector mesons. The non-saturation of the strangeness (and anti-strangeness) production shows that novel non-equilibrium production processes arise in these reactions. Finally, the centrality dependence of J/ψ absorption in $Pb+Pb$ collisions presents further hints towards the non-equilibrium nature of such reactions.

Is there evidence for the long sought-after quark-gluon plasma that thus far has only existed as a binary array of predictions inside teraflop computers?

As we will discuss, it is too early to tell definitely – notwithstanding the combined results of the CERN-SPS program as announced in February 2000.

Theoretically there are still too many "scenarios" and idealizations to provide a satisfactory answer. Recent results from microscopic transport models as well as macroscopic hydrodynamical calculations differ significantly from predictions of simple thermal models, e. g. in the flow pattern. Still, these non-equilibrium models provide reasonable predictions for the experimental data. We may therefore be forced to rethink our concept of what constitutes the deconfined phase in ultra-relativistic heavy-ion collisions. Most probably it is not a blob of thermalized quarks and gluons. Hence, a quark-gluon plasma can only be the source of *differences* to the predictions of these models for hadron ratios, the J/Ψ meson production, dilepton yields, or the excitation function of transverse flow. And there are experimental gaps such as the lack of intermediate mass $A \approx 100$ data and the still limited number of beam energies studied thus far, in particular between the AGS and SPS. In the meantime, the field is at the doorstep of the next milestones: $A+A$ at $\sqrt{s} = 30-200$ AGeV has begun at RHIC/BNL in 2000, while the SPS (and the planned GSI-SIS/200) program continues to investigate the lower energy range $\sqrt{s} = 6-12$ AGeV (30-80 AGeV in the laboratory frame).

Organization of this review

This review is organized as follows: We first introduce and discuss two Non-equilibrium models used in the investigation of ultra-relativistic heavy ion collisions, the 3-fluid hydrodynamical model and the UrQMD hadronic transport model. Then we present nuclear stopping power as a fingerprint of the creation of compressed hadronic matter. We discuss flow signatures as probes of the pressure reached in the fireball, and particle spectra and ratios as probes of temperature and chemical properties of the fireball. As strong hints at the transient existence of deconfined quark matter, we review strangeness enhancement and the ideas of strangelets and hypermatter. As a further possible signal of the quark-gluon plasma, we then discuss the suppression of

the J/ψ. Dileptons are presented as the (next to direct photons) unique probe to look directly at the heart of the fireball, and the experimental results and their interpretation are reviewed. We conclude our presentation with an outlook at the possible end of short distance physics and the predictive power of QCD: the conceivable creation of black holes due to the effects of large extra dimension in heavy ion collisions at the planned LHC machine.

NON-EQUILIBRIUM MODELS FOR THE STUDY OF ULTRA-RELATIVISTIC HEAVY ION COLLISIONS

In the present survey we employ two sharply distinct non-equilibrium models for relativistic heavy ion collisions, namely the macroscopic 3-fluid hydrodynamical model [1] and the Ultra-relativistic Quantum Molecular Dynamical model, UrQMD [2].

The first model assumes that a projectile- and a target fluid interpenetrate upon impact of the two nuclei, creating a third fluid (in the present version baryon free, see, however, [3]) via new source terms in the continuity equations for energy- and momentum flux. Those source terms are taken from energy- and rapidity loss measurements in high energy pp-collisions. The equation of state (EoS) of this model assumes equilibrium only in each fluid separately and allows for a first order phase transition to a quark gluon plasma in fluid 1, 2 or 3, if the energy density in the fluid under consideration exceeds the critical value for two phase coexistence. Pure QGP can also be formed in every fluid separately, if the energy density in that fluid exceeds the maximum energy density for the mixed phase.

The UrQMD model, on the other hand, assumes an independent evolution of hadrons, strings, and constituent quarks and diquarks in a non-equilibrium multi-particle system. The collision terms in this system of coupled Boltzmann equations (partial differential/integral equations) are taken from experimental data, where available, and otherwise from additive quark model and string phenomenology.

What is the role of partonic degrees of freedom in heavy ion reactions at the SPS?

Fig. 1 shows the time evolution of the energy density ε in central $Pb+Pb$ reactions at 160 AGeV as obtained within *a)* the parton cascade approach VNI [4], *b)* the UrQMD model [5]. It can be seen that in both models and at early times of the collision, a large fraction of the energy density is contained in partonic degrees of freedom (VNI) or to nearly equal parts in constituent diquarks and quarks from the strings and in virtual hadrons. This (virtual) "partonic" phase in $Pb+Pb$ reactions at 160 AGeV is, however, not to be identified with an equilibrated QGP. Note that the absolute values differ by a factor 2 in the two models and depend heavily on the rapidity cuts imposed to discriminate between virtual free streaming and interacting matter.

A sharp transition from a partonic state to the hadronic phase can be described within a non-relativistic, classical microscopic framework [6], as shown in Fig. 2. The critical temperature here is determined by the strength of the quark color potential.

This model, the quark molecular dynamics (qMD) [7], can be used to investigate the detailed hadronization dynamics from a hot and dense system of quarks to a gas of baryonic resonances, baryons and mesons.

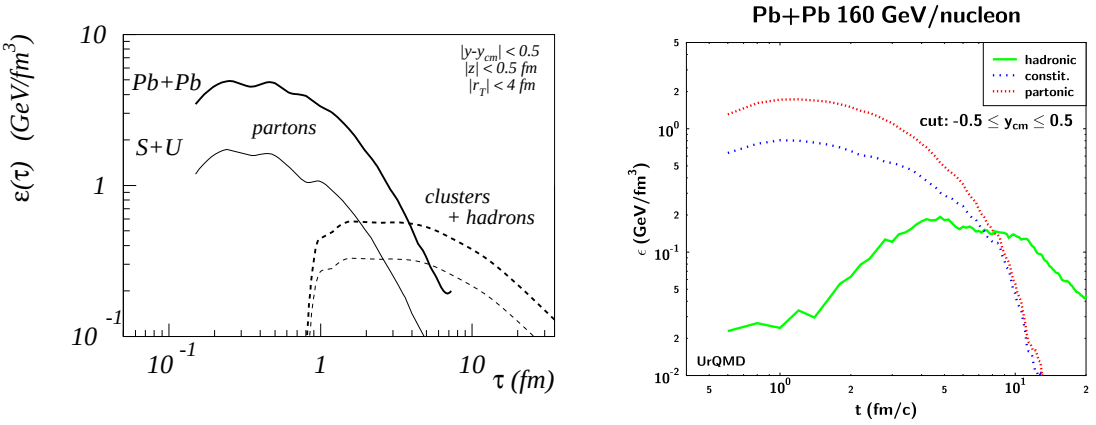

FIGURE 1. (Left:) Parton cascade (VNI, from [4]) and (Right:) UrQMD results for the time evolution of energy density in central $Pb+Pb$ reactions at 160 AGeV. At an early stage, most of the energy is contained in the partonic degrees of freedom (VNI) or in constituents (UrQMD).

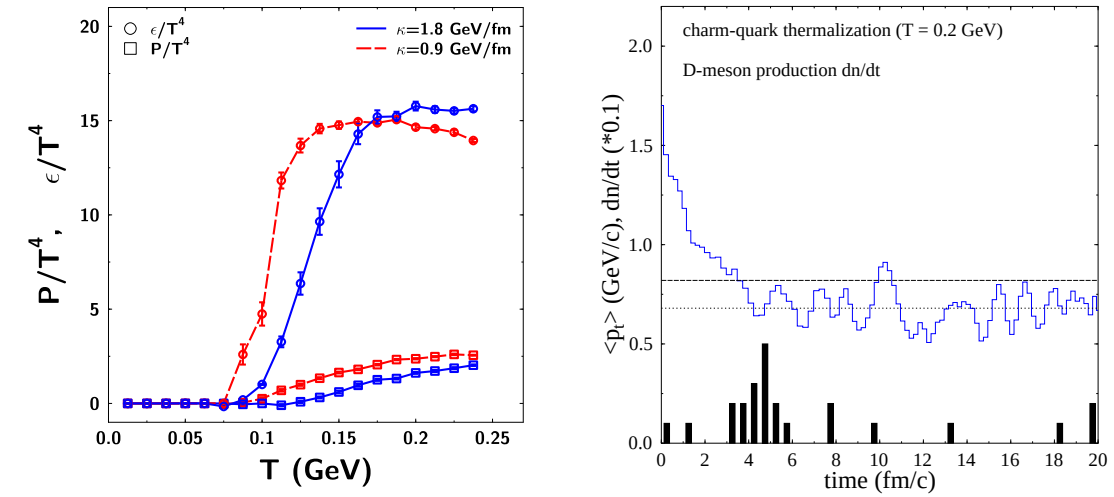

FIGURE 2. (Left) Energy density and pressure in a multi quark system interacting via a linear potential. (Right) D meson formation in the same model, showing charm quark thermalization.

CREATION OF COMPRESSED HADRONIC MATTER: NUCLEAR STOPPING POWER.

To study the properties of highly excited hadronic or quark gluon matter, normal nuclear matter has to be strongly compressed or heated. How is this possible? The answer was proposed 30 years ago [8, 9]: With high-energy nucleus-nucleus collisions. The idea was that the occurrence of multiple collisions converts longitudinal momentum into transverse momentum and secondary particles, leading to the creation of a zone of high energy density. Nuclear shock waves have been suggested as a primary mechanism of creating high energy densities in collisions with $\sqrt{s} \leq 20$ GeV [8, 9, 10]. The resulting

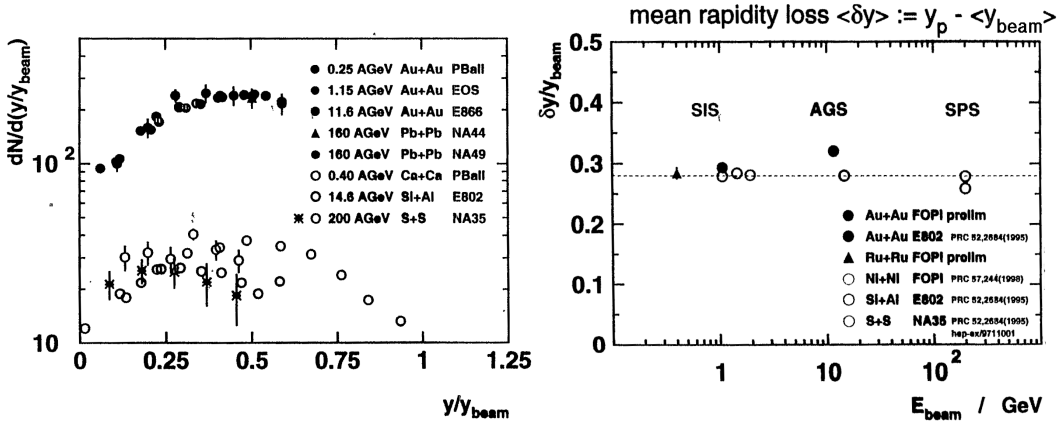

FIGURE 3. Left: Scaled rapidity $dN/d(y/y_{beam})$ distribution as a function of scaled rapidity (y/y_{beam}). Right: Mean rapidity loss versus beam energy. At SIS, AGS and SPS energies. Figure taken from [18].

energy density should be high enough to produce a state of high density resonance matter [9, 11, 12] or even a quark-gluon plasma [13]. For CERN SPS energies estimates for the achieved energy density at proper time $\tau_0 \approx 1\text{fm/c}$ are of the order $\varepsilon \approx 1 - 5\text{GeV/fm}^3$. Extrapolations to BNL RHIC energies suggest that energy densities up to 20 GeV/fm^3 at $\rho \approx 2\rho_0$ may be reached.

The degree of stopping the incident nucleus suffers, when colliding with another nucleus (*nuclear stopping power*) manifests itself in a shift of the rapidity-distributions of the incident nucleons towards mid-rapidity. That means: The shape of the baryon rapidity distribution can give clear indications on the degree of stopping and the onset of critical phenomena. Due to the strong dependence of the baryon rapidity distribution on the baryon–baryon cross section [14, 15, 16], a rapid change in the shape of the scaled $dN/d(y/y_p)$ distribution with varying incident beam energy is a clear signal for new degrees of freedom which show up during the reaction (i.e. deconfinement), e.g. due to phenomena such as critical scattering [17]. The width of the $dN/d(y/y_p)$ distribution for baryons is inversely proportional to their cross section.

As an example on the left of figure 3 the measured scaled rapidity $dN/d(y/y_{beam})$ distribution as a function of scaled rapidity (y/y_{beam}) is shown for several collision systems at various energies. One observes a clear dependence of the shift in the scaled rapidity distribution on the collision systems. For the large Systems (Au+Au, Pb+Pb) a significant shift occurs, i.e. strong stopping power is observed, while for the smaller systems (e.g. Ca+Ca) only little stopping occurs. That means: Large systems are best suited for the creation of a zone of very high energy density. This is because during the collision of large systems more collisions occur and therefore the incident nucleons lose more energy that is deposited in the central reaction zone. This finding is independent of the collision energy. Figure 3 (right) shows the mean rapidity loss versus beam energy. It stays constant in the shown energy region.

The experimental situation can be summarized as follows: At AGS and SPS an extensive investigation of the nuclear stopping power is near completion. Proton-proton [19] and peripheral nucleus-nucleus interactions at AGS [20, 21] and SPS [22] energies

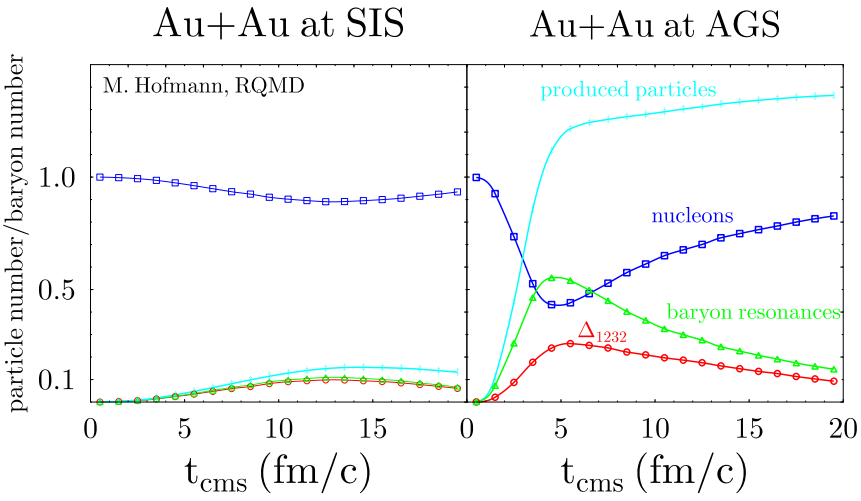

FIGURE 4. Time evolution of particle multiplicities (scaled with the number of incident nucleons) for central Au+Au collisions at 1 GeV/nucleon (SIS) and at 10.6 GeV/nucleon (AGS). At SIS energies, only about 10% of the nucleons are excited to resonances whereas at AGS energies the degree of excitation exceeds 50%. For a time-span of up to 10 fm/c the baryons are in a state of $\Delta-$matter. The figure has been taken from [25].

yield a forward–backward peaked dN/dy distribution in the C.M. frame, and a low degree of baryon stopping. A higher degree of stopping is observed for central collisions of intermediate mass nuclei (Si+Si at AGS, S+S at SPS): The rapidity distribution is flat at C.M. rapidities, two broad bumps are observed between projectile/target and C.M. rapidities respectively [20, 21, 22]. The heaviest collision systems (gold and lead respectively) exhibit the largest stopping power and thus correspond to the creation of the highest baryon densities: The form of the measured baryon rapidity distributions shows experimentally that the central rapidity region up to $E_{lab} \sim 200$ GeV/nucleon is not net-baryon free, in contrast to what had been expected in most early papers. Rather strong stopping as assumed first in hydrodynamic model studies [23, 24] is observed. Therefore, results of theoretical analyses, which rely heavily on a net-baryon free mid-rapidity region with zero baryo-chemical potential have to be taken with care. The quantitative measurements of the A-dependent stopping of baryons is one of the most important results of the AGS and SPS measurements. In summary, the experimental results demonstrate that highly excited dense matter is formed at mid-rapidity. They prove that a new state of elementary matter has been created.

What are the properties of this new state of matter? Hadronic transport model calculations indicate that the excited state of baryonic matter is dominated by the Δ_{1232} and other baryon resonances, i.e. the deposited energy in the central rapidity region is mainly transformed into these new degrees of freedom. E.g. for central Au+Au collisions at AGS a long apparent lifetime ($>$ 10 fm/c) and a rather large volume (several hundred fm^3) for this resonance-matter state [25] (see figure 4) is predicted.

The energy densities of $\varepsilon \approx$ 3-20 GeV/fm^3 estimated for SPS and RHIC indicate that part of the system may have entered the predicted state of deconfinement [18]. However,

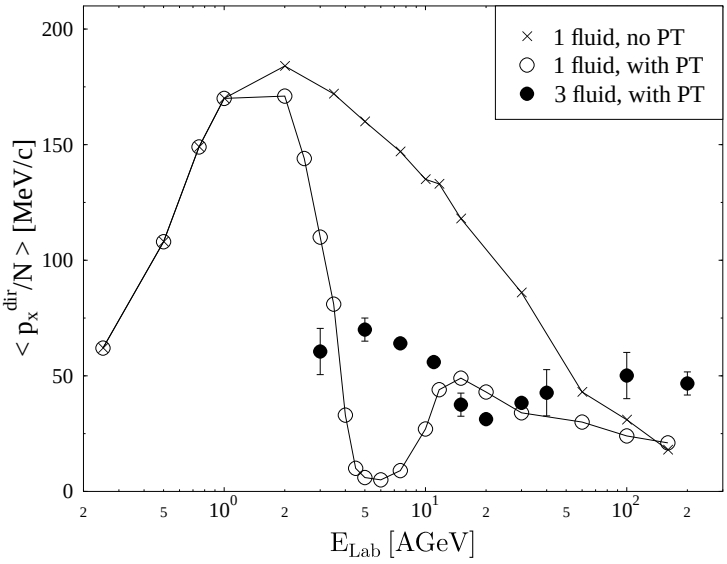

FIGURE 5. The excitation function of transverse flow as obtained from one fluid hydrodynamics with (open circles) and without (crosses) a first order phase transition[31], and the results of the three-fluid hydrodynamical model (filled circles). The drop of p_x due to the softening of the EoS is shifted to $E_{\rm lab} \approx 20$ AGeV.

hadronic transport models predict or reproduce the measured rapidity distributions, if baryon and meson rescattering and particle production via string decay [26, 27, 28, 29, 2] are included. Also hadronic models which include multi–quark droplets [30] above $\varepsilon_{\rm crit}$ seem to give similar results. Therefore up to now, the inclusive central distributions do not give a clear and decisive answer to the question of whether this matter is predominantly of hadronic or quark nature. The inclusion of string excitations, collisions and decays are a first step towards modeling the parton/quark substructure of hadrons. These models go beyond what one would term purely hadronic model and should give more insight in the structure and properties of the matter in the highly compressed and heated central interaction zone of high energy nucleus-nucleus collisions.

FLOW SIGNATURES: PROBING THE PRESSURE OF THE FIREBALL

Collective Flow and the softening of the EoS

The excitation function of collective transverse flow is the earliest predicted signature for probing compressed nuclear matter. Transverse collective flow depends directly on the pressure $p(\rho, S)$, i.e. the EoS. The flow excitation function is sensitive to phase transitions [23] by a collapse of the directed transverse flow [32, 33]. This is commonly referred to as *softening* of the EoS [31].

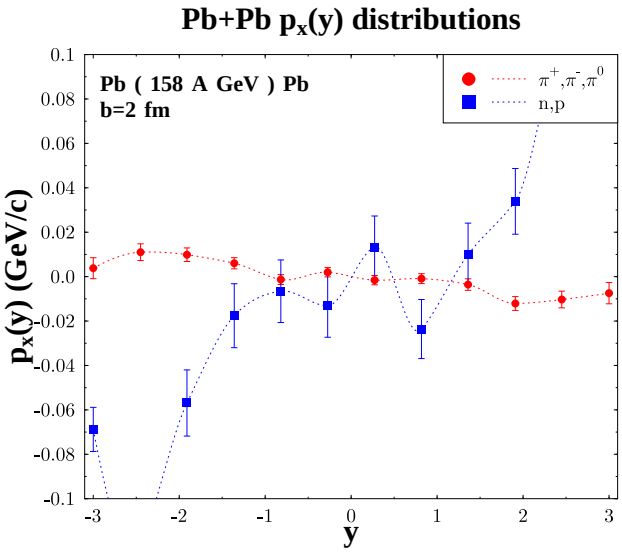

FIGURE 6. Theoretical predictions for transverse collective flow in $Pb+Pb$ collisions as obtained with the microscopic UrQMD transport model.

An observation of a local minimum in the excitation function of the transverse directed flow would thus be an unambiguous signal for a first order phase transition in dense matter. It's experimental measurement would serve as strong evidence for a QGP, if that phase transition is of first order.

Recent calculations within three-fluid hydrodynamics [34] show a shift in the drop of transverse flow to higher energies, $E_{\rm lab} \approx 20$ AGeV, see Fig. 5. Experimentally, the recent discovery of proton flow and pion anti-flow at the SPS is in line with UrQMD and RQMD predictions (Fig. 6, and [35]).

Let us now discuss the results obtained from hadronic probes, such as observed particle ratios transverse momentum spectra and ratios, enhancement of strange baryons, light mesons, and production of J/Ψ.

Observed hadrons include feeding by the decay of resonances.

PARTICLE SPECTRA AND RATIOS: PROBING THE THERMAL AND CHEMICAL PROPERTIES OF THE FIREBALL

Thermal or statistical interpretations of the particle production in high energy collisions of elementary particles and heavy ions have been carried out for a long time [36, 37, 38, 39, 40, 41, 42, 43]. In the case of heavy-ion collisions a range of particle ratios measured at SIS, AGS, SPS and now also RHIC for different energies and different colliding systems have been fitted with a noninteracting gas calculation. The measured ratios reflect the relative particle numbers at the point of chemical freeze-out, i.e. the point when inelastic collision cease and therefore the chemical composition of the system is

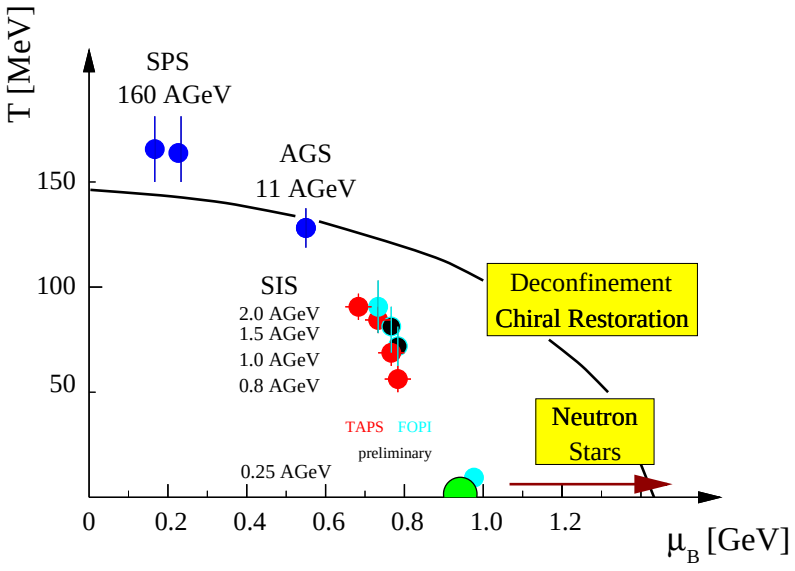

FIGURE 7. Freeze-out curve for different collision systems at various energies as obtained from ideal gas fits [44].

not changed anymore. E.g. noninteracting gas fits yield a chemical freeze-out curve in the $T-\mu$ plane (see fig 7,[44]).

The measured particle spectra can be connected to the thermal or kinetic freeze-out, i.e. the point when no more elastic collisions occur.

The underlying model is as follows: One assumes a thermalized system with a constant density $\rho(r)$ (box profile), a constant temperature $T(r)$ and a linear radial and longitudinal flow velocity profile $\beta_{\perp}(r)$, $\beta_{||}(r)$. These parameters are assumed to be the same for all hadrons/fragments. At some time $t^{\text{break-up}}$ and density $\rho^{\text{break-up}}$, the system decouples as a whole (a horizontal freeze-out in the $T(z)$-plane) and the particles are emitted instantaneously from the whole volume of the thermal source. A complete loss of memory results, due to thermalization – the emitted particles carry no information about the evolution of the source. If one wants to use the inverse slope parameter T as thermometer [23], the feeding from Δ's etc., as well as the radial flow need to be incorporated into the analysis. The same holds for the use of d/p, π/p etc. as an entropymeter[45]. In addition, the proper Hagedorn volume correction can be applied [46]. A two parameter fit (μ_q, T, μ_s is fixed by strangeness conservation) to the hadronic freeze-out data describes the experimental results well, if feeding is included (see e.g. [44]). The particle multiplicities at the chemical freeze-out are calculated using an ideal gas approach, i.e. all particles are on mass-shell. Does this compatibility with a thermal source proof volume emission from a globally equilibrated source? Are the obtained temperatures and chemical potentials unique or strongly model dependent? How do interactions change the deduced freeze-out values?

The values for T and μ_{B} that were obtained using the ideal gas analyses of particle ratios can be used as input for a $SU(3)$ chiral mean-field model [47] extended to finite temperatures [48]. This model self-consistently contains scalar and vector interactions

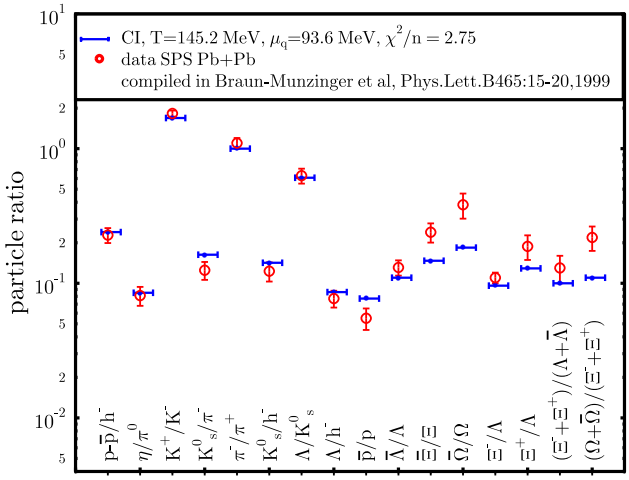

FIGURE 8. Fit of hadron ratios from the chiral model with a first order phase transition (CI) to data from $Pb+Pb$ collisions at SPS. The obtained values of T and μ allow the prediction of further ratios. T is much lower than results from the ideal hadron gas approach.

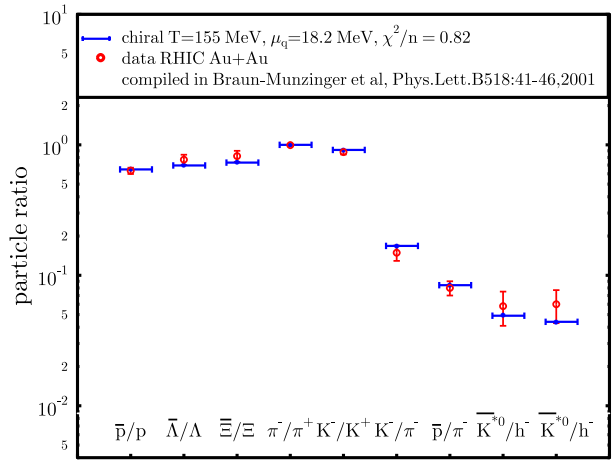

FIGURE 9. Fit of hadron ratios from the chiral model to data from $Au+Au$ collisions at RHIC.

that change the properties of the hadrons in the medium. Furthermore the model shows a transition to a chirally restored phase. The nature of this transition in the model depends on the included degrees of freedom and the chosen parameters [49]. Feeding from the decay of higher resonances is included. One finds that in such a model with a first order phase transition the ideal gas model values $T = 168$ MeV and $\mu_B = 266 MeV$ [44] lead to strong deviations from the experimental data and one has to re-fit the T and μ values. The obtained values for SPS Pb+Pb at SPS are: $T \approx 145$MeV and $\mu_B \approx 281$MeV.

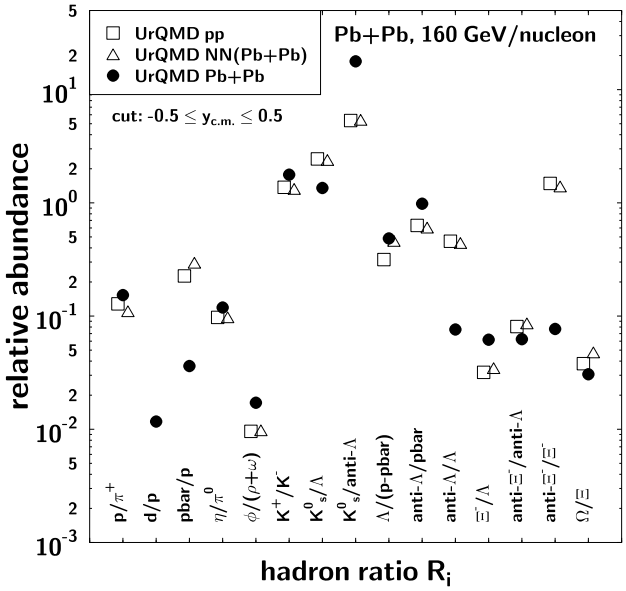

FIGURE 10. UrQMD prediction for hadron ratios in $Pb+Pb$ collisions at mid-rapidity (full circles), compared to a superposition of pp, pn and nn reactions with the isospin weight of the $Pb+Pb$ system (open triangles), i.e. a first collision approach.

While the chemical potential is nearly unchanged due to the interactions, a decrease of $\Delta T \approx 20$MeV in the temperature results. Furthermore the analyses shows that no fit is possible above the phase transition temperature, what is realistic, since above T_C the particle densities are very high and the system is not dilute at all. Using the re-fitted T, μ values, the hadronic chiral model satisfactorily reproduces the measured particle ratios for Pb+Pb at SPS (fig. 8). The larger χ^2/n value is caused by the neglect of final weak interactions, as has already been shown by [50].

For RHIC the situation is similar: Ideal gas analyses yield freeze-out temperatures in the range of $T = 160 - 180$MeV, the chiral model with a first order phase transition yields $T \approx 150$MeV. The baryon chemical potential μ_B in both cases is around 40MeV. The agreement between data and calculated ratios is even improved, as can be seen from fig. 9.

Other parameterizations of the chiral model yield different T, μ_B values, but comparable quality of the fits [51]. That means: Not only ideal gas models, but also equilibrium models which account for the interactions in the hot and dense central region of relativistic heavy ion collisions can reproduce the measured particle ratios. The obtained chemical potentials seem to be robust but the temperatures strongly depend on the used model. This has also been shown in [52]. Therefore one must conclude that the extracted freeze-out values from different thermal and chemical equilibrium approaches are not unique but strongly model dependent.

The microscopic UrQMD transport model is in good agreement with the measured hadron ratios of the system $S+Au$ at CERN/SPS [53]. A thermal model fit to the calculated ratios yields a temperature of $T = 145$ MeV and a chemical potential of $\mu_B = 165$ MeV. However, these ratios exhibit a strong rapidity dependence. Thus,

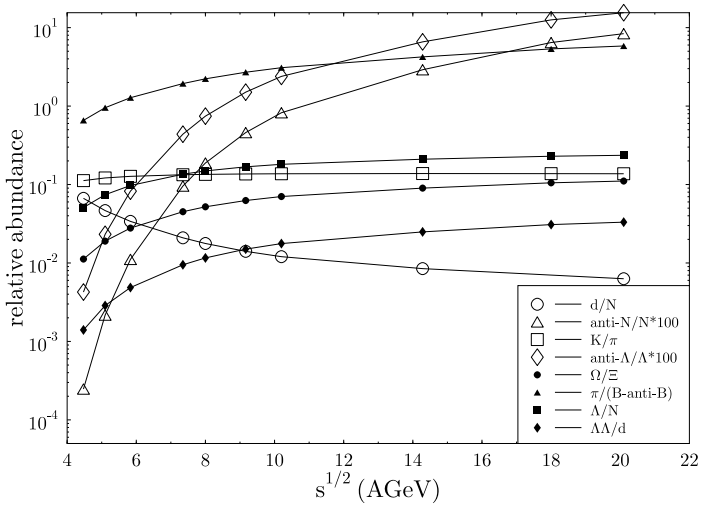

FIGURE 11. The excitation function of various particle ratios as calculated from the S/A values obtained from the three-fluid model. Feeding due to decays of resonances is taken into account.

thermal model fits to data may be distorted due to different acceptances for the individual ratios.

Hadron ratios for the system $Pb+Pb$ are predicted by UrQMD and can be fitted by a thermal model with $T = 140$ MeV and $\mu_B = 210$ MeV (Fig. 10). Analyzing the results of non-equilibrium transport model calculations by an equilibrium model may, however, be not meaningful.

There is a problem in the definition of equilibrium in itself: Do heavy ion collisions ever reach a thermalized system? Or are there transient steady states off equilibrium [54]? Due to the rapid dynamics of the system, the assumption of detailed balance is not fulfilled in the initial stage. This drives the system into a steady state far from equilibrium, but stationary in time. This steady state is easily visible in an enhanced production of light mesons, as compared to thermal models.

During the initial off-equilibrium stage of energetic nuclear collisions, a large amount of entropy can be produced [10]. The subsequent expansion is, on the other hand, often assumed to be nearly isentropic. The entropy produced during the compression stage is closely linked to the finally observable relative particle yields.

This entropy production can be calculated [55] within three-fluid hydrodynamics. The entropy per net participating baryon, S/A, saturates rapidly as a function of CM-time and is essentially time independent for later times when the freeze-out is reached. The chemical composition of the fireball is given by the net baryon density, the net (zero) strangeness of the system, and the specific entropy S/A, as described for the thermal model above.

The hadron ratios thus obtained are shown in Fig. 11. At AGS and SPS energies, they are quite close to the data [56, 54]. For such a simple estimate of hadron production in

nuclear collisions, deviations from the experimental ratios by up to factors of two have to be expected. Nevertheless, it is clear from Fig. 11 that the simultaneous measurement of various hadron ratios, like $\pi/\left(B-\overline{B}\right)$, d/N and, in particular, $\overline{B}/B$ (provided antibaryons also reach chemical equilibrium) allows to determine the produced entropy in the energy range between the AGS and the SPS. In contrast, the K/π-ratio is practically constant. The total specific entropy S/A produced within the three-fluid model is consistent with the S/A values extracted from data using relative particle yields from the thermal model. One finds $S/A = 11$ for AGS and $S/A = 38$ for SPS energies.

The excitation function of the specific entropy $S/A(\sqrt{s})$ does not exhibit any threshold signatures of the phase transition to the QGP incorporated in the EoS. This is due to the gradual transition through the wide coexistence region in the energy density between $E_{\mathrm{lab}} \approx 10$–$100$ AGeV.

STRANGENESS ENHANCEMENT: HINTS AT DECONFINED QUARK MATTER.

Let us now turn to multi-strange signals. In nucleon nucleon collisions, the production of particles containing strange quarks is strongly suppressed as compared to the production of particles with u and d quarks due to the higher mass of the $s\bar{s}$ quark pair [57]. It has been speculated that the yield of strange and multi-strange mesons, (anti-) baryons and anti-hyperons (Λ, Σ, Ξ and Ω) should be enhanced in the presence of a QGP. This can be understood as follows. The strangeness production rate is described by the Schwinger-factor [57] as long as no chemical equilibrium has been reached. This factor shows a mass dependence like $A\exp(-km_q)$, where A and k are some constants and m_q is the quark mass. So the production of heavier quarks like the strange quark is strongly suppressed compared to that of light quarks. On the other hand if the system can reach chemical equilibrium, the yield of different quarks and anti quarks are almost the same. It is now believed that the QGP-phase exists long enough for the chemical equilibrium to establish, so up, down and strange quarks reach a similar ratio. However if no QGP is produced, the chemical equilibrium of the hadronic phase has a much lower strangeness content. So the idea is that one can distinguish the production of a hadronic phase from the QGP phase by looking at the strangeness of the produced particles.

However only the end of the whole process is observable. To be able to interpret high strangeness ratio as a QGP signal it has to be supposed that matter passes through the hadronic phase fast enough to make equilibration impossible. Only than it is possible to discern the QGP production from the production of a hadron phase.

The study of (multi)strange hyperons by the WA97 [58] and the NA49 collaborations show an enhancement of strangeness production for central collisions when studying the centrality dependence of various strange particle yields (Λ, Ξ, Ω) in $Pb+Pb$ collisions at 158 AGeV as compared to $p+Pb$ collisions at 158 AGeV. The centrality is given as the extrapolated number of participant nucleons N_{part}. We propose as centrality variable the number of produced pions N_{π^-}. N_{part} shows a nonlinear behavior with the volume of the participant zone, while N_{π^-} shows perfect participant scaling. Scaling has been observed for central collisions ($N_{\mathrm{part}} \geq 100$).

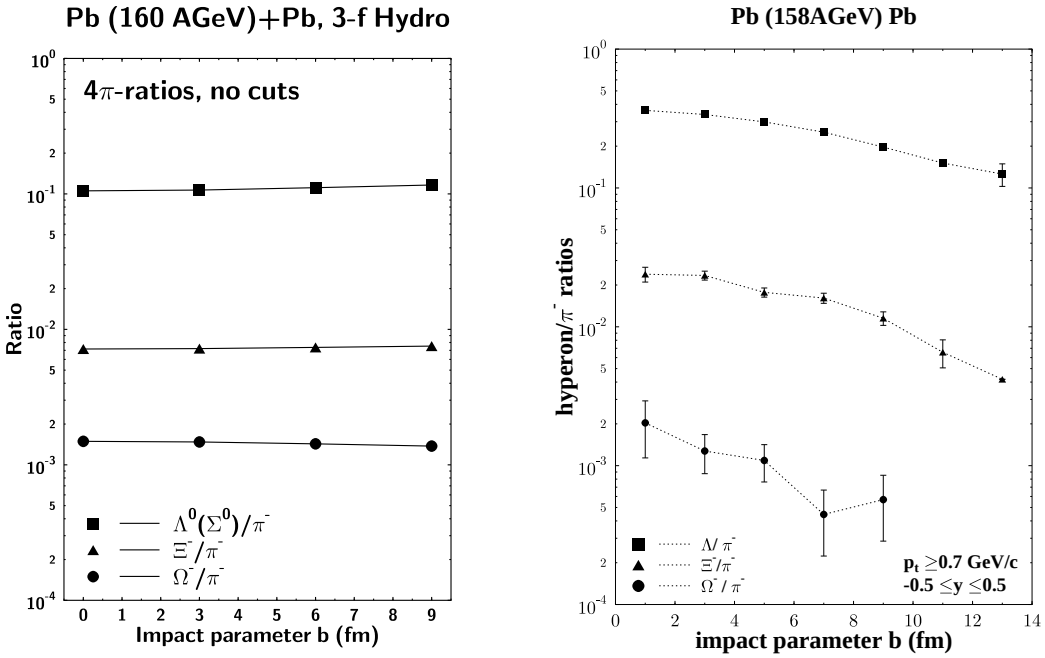

FIGURE 12. Hyperon to π^- ratio as a function of impact parameter *b*, as obtained from the three-fluid hydrodynamical model (left) and the UrQMD model (right). In the UrQMD model, the observed strangeness enhancement is already a natural consequence of ordinary hadronic rescattering.

The UrQMD calculations (Fig. 12, right) show scaling. The hyperon to π^- ratio is depicted in Fig. 12 (right) as a function of impact parameter *b*. For central collisions, all ratios change only moderately, thus an approximate linear scaling of the hyperon yield with pion number N_{π^-} is observed. For peripheral collisions, the ratios decrease. The ratios vary with a factor of 2 to 5 for different impact parameters depending on the hyperon and its strangeness content. The three-fluid hydrodynamical model with an EoS with a first order phase transition to a QGP yields constant ratios (Fig. 12 left). Note the substantial differences in the Ξ/π-ratios between the two predictions. The QGP which will be created at AGS, RHIC or SPS energies will most likely be characterized by non-zero chemical potential μ_d and mu_u. This will cause an increase in the densities of u and d quarks with respect to the densities of the s and $\bar{s}$ quarks. Due to the increase of the density of the u and d quarks, or the decrease of the s and $\bar{s}$ quarks, the $\bar{s}$ quarks are more likely to combine with u or d quarks. And similarly s quarks combine with $\bar{u}$ or $\bar{d}$. There will be a change in the ratio of $K^{\mp}/\pi$ during the QGP case.

The strangeness fugacity γ_s is introduced in thermo-chemical approach to account for incomplete chemical equilibration. It has been also compared to the measured ratios and the connected thermo-dynamical variables with a hadron gas scenario or a QGP scenario with some hadronization. However there are some certain drawbacks. One is the strange particle abundances after freeze out, are very close to those of the fully equilibrated

hadron gas at the same entropy content. The reason can be explained by the volume of the hadron gas of the same total energy which must be larger due to the smaller number of available degrees of freedom. As a result one expects that the abundance of strange quarks is diluted during the hadronization process. This effect can be seen in many hadronization models. The computation of particle abundances in the QGP and the hadron gas scenario are mostly based on the assumption of chemical and thermal equilibrium. However for the hadronic case these assumptions cannot be justified since it has been shown that the strangeness equilibration time exceeds the reaction time of a heavy ion collision by at least one order of magnitude.

Strangeness production in the hadronic scenario is a non-equilibrium process. During the pre-equilibrium stages, typical longitudinal momenta are much higher than in the case of a thermal momentum distribution which leads to enhanced strangeness production. It's final "equilibrium" temperature is therefore only partly connected to the measured strange particle yields and spectra.

STRANGELETS AND HYPERMATTER

The observed abundant production of strange baryons at AGS and SPS energies led people to speculate about implications for hypermatter (multi-hyperon clusters or strange quark droplets) formation [59, 60, 61, 62, 63]. Speculations about the existence of such objects, with baryon numbers $B > 100$, have been around for decades, in particular within astrophysics. Such states are allowed for by the standard model, although so far their existence has not been proven in nature, e.g. in the form of strange neutron stars. *Quark matter* systems with $A > 1$ are unstable, if they only consist of *u* and *d* quarks, due to the large Fermi energy of these non-strange quarks. The system's energy may be lowered by converting some of the *u* and *d* quarks into *s* quarks (i.e. introducing a new degree of freedom). The energy gain may over-compensate the high mass of the *s* quarks and thus strange quark matter (SQM) may be absolutely stable [62]. Hadrons with $B > 1$ and $S < 0$ have been considered even before the advent of QCD [59, 60]. However, first the development of the MIT Bag Model [64] allowed to model such states. Long hypermatter lifetimes (for hundreds of quarks and a strangeness per baryon ratio in the order of one) have been predicted, up to 10^{-4} seconds [61]. Further detailed investigations of small pieces of strange quark matter, so called *strangelets*, reveal possible (meta)stability for $B > 6$ [62, 63]. Figure 13 shows possible creation scenarios for strangelets and strange nuclei. The right hand side shows the clustering of strange baryons to strange nuclei, while the left hand side shows the distillation of strange quark matter from a quark gluon plasma.

The simplest *strangelet* is the $H-$dibaryon with zero charge, $B = 2$ and $S = -2$, which consists of $2u, 2d$ and $2s$ quarks, followed by the *strange quark–α* with $6u, 6d$ and $6s$ quarks [62, 65]. For a QGP – hadron fluid first order phase transition with nonzero baryo-chemical potential, a mechanism analogous to associated kaon-production yields an enriched population of *s* quarks in the quark-gluon phase, while the $\bar{s}$ quarks drift into the hadron phase [66, 67]. This strangeness separation results in the distillation of metastable *strangelets* only if the Bag constants are very small, $B < 180$ MeV/fm^{-3}

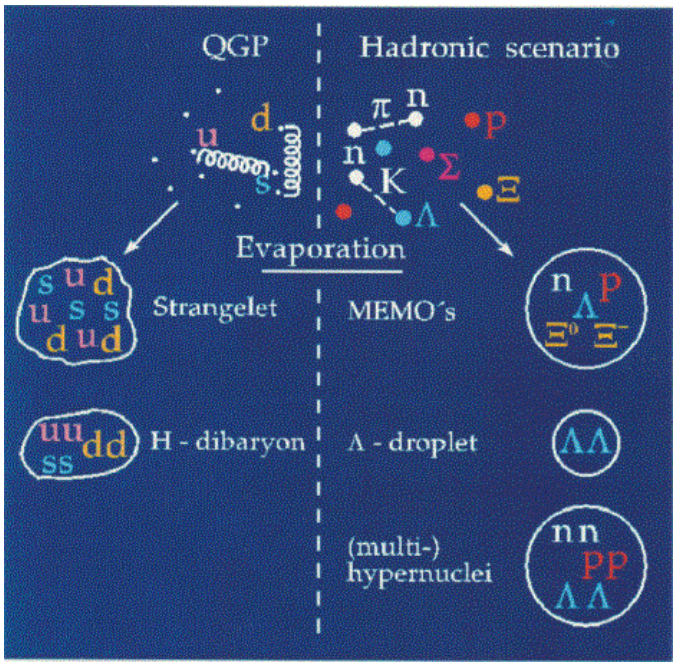

FIGURE 13. Possible formation scenarios for strange matter. The left hand side shows the formation of strange quark matter from the quark gluon plasma. The right hand side shows the clustering of strange baryons to strange nuclei

[66]. Experimentally *strangelets* are distinguishable from normal nuclei due to their very small or even negative charge to mass ratio. The most interesting candidates for long-lived *strangelets* are lying in a valley of stability which starts at the *quark–α* and continues by adding one unit of negative charge, i.e. (A,Z)=(8,-2),(9,-3)…[68]. Recent calculations indicate that positively charged *strangelets* seem only to exist for $A > 12$ and very low bag parameters [68]. There exist, however, other forms of hypermatter with similar properties as *strangelets*: hyperclusters or MEMO's (metastable exotic multi-hyperon objects) consist of multiple Λ, Σ and Ξ hyperons [69], and possibly also nucleons. The double-Λ hypernucleus ${}^{6}_{\Lambda\Lambda}$He has been observed long ago [70]. Properties of MEMOs have been estimated using the Relativistic Mean Field model. MEMOs can contain multiple negatively charged hyperons, therefore they may also have zero or negative charge-to-mass-ratios.

MEMOs or hyperclusters could form a doorway state to *strangelet* production, or vice versa: MEMOs may coalescence in the high multiplicity region of the reaction. If strangelets are stronger bound than "conventional" confined MEMOs, the latter may transform into *strangelets*. The cross sections for production of MEMOs in relativistic heavy ion collisions rely heavily on model parameters (e.g. in the in the coalescence model p_0 and r_0). The predicted yields are typically $< 10^{-8}$ per event [69, 71].

Strangelet searches are underway at the AGS [72, 73, 74] and SPS [75, 76, 77, 78, 79]. So far no long lived ($\tau > 10^{-7}$ s) *strangelets* have been unambiguously identified – the upper limits for the production cross sections established by the experiment are still consistent with theoretical predictions for short lived MEMOs since they cannot

be tested in the present long flight path experiments. There has been a report of one candidate with $Z = -1$, $N/Z = 7.4$ GeV and $\tau > 85\ \mu s$ [79, 77, 80]. Therefore this exciting topic awaits more experimental effort.

Current experiments are designed to detect *strangelets* with a small charge-to-mass ratio and rather long lifetime ($\tau \geq 12\ \mu s$ in the case of [77, 78]). The present experimental setups are hardly sensitive to the most promising long-lived and negatively charged *strangelet* candidates beyond the *strange quark–*α. Unfortunately, plans for extending experiment E864 at the AGS to look for highly charged strangelets with $B > 10$ could not be followed because the AGS fixed target heavy ion program was put to rest.

Future experiments at collider energies (STAR at RHIC and ALICE at LHC) will be sensitive for short-lived metastable hypermatter, too [81, 82, 83].

J/ψ SUPPRESSION: A CLEAR SIGNAL OF THE QGP?

Debye screening of heavy charmonium mesons in an equilibrated quark-gluon plasma may reduce the range of the attractive force between heavy quarks and antiquarks [84]. Mott transitions then dissolve particular bound states, one by one. NA38 found evidence of charmonium suppression in light ion reactions. Then also in $p+A$ such suppression was observed. New preliminary $Pb+Pb$ data of NA50 show "anomalous" suppression.

One of the main problems in the interpretation of the observed suppression as a signal for deconfinement is that non-equilibrium dynamical sources of charmonium suppression have also been clearly discovered in $p+A$ reactions, where the formation of an equilibrated quark-gluon plasma is not expected. A recent development is the calculation of the hard contributions to the charmonium- and bottonium-nucleon cross sections based on the QCD factorization theorem and the non-relativistic quarkonium model [85]. Including non-perturbative contributions, the calculated $p+A$ cross section agrees well with the data. Whereas these descriptions of nuclear absorption can account for the $p+A$ observation, the corrections needed for an extrapolation to $A+A$ reactions are, however, not yet under theoretical control.

Purely hadronic dissociation scenarios have been suggested [88, 89, 90] which could account for J/ψ and ψ' suppression without invoking the concept of deconfinement ("comover models"). Suppression in excess to that due to preformation and nuclear absorption is ascribed in such models to interactions of the charmonium mesons with "comoving", but probably off-equilibrium, mesons and baryons, which are produced copiously in nuclear collisions. Fig. 14 shows an UrQMD calculation which employs a microscopic free streaming simulation for J/ψ production and a microscopic transport calculation for nuclear and comover dynamics as well as for rescattering [87]. The dissociation cross sections are calculated using the QCD factorization theorem [85], feeding from ψ' and χ states is taken into account, and the $c\bar{c}$ dissociation cross sections increase linearly with time during the formation of the charmonium state. Taking into account the non-equilibrium "comovers" ($\sigma_{meson} \approx 2/3\sigma_{nucleon}$), the agreement between theory and data is reasonable (Fig. 14). New, unpublished data agree better with the model predictions, but the high and low E_{T} regions remain to be studied carefully in the experiment. At present, no ab initio calculation does predict sudden changes in

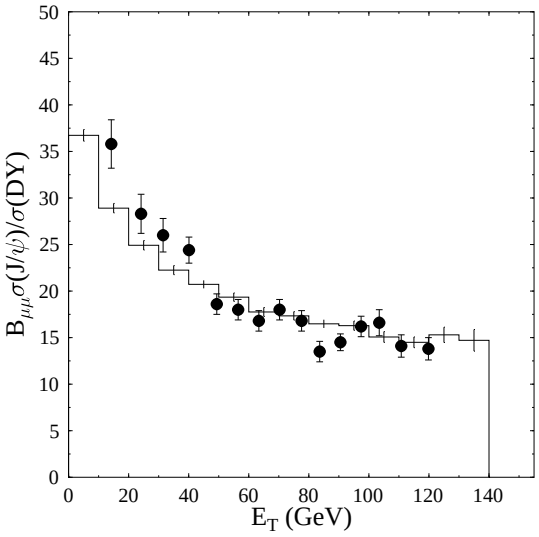

FIGURE 14. The ratio of J/ψ to Drell-Yan production as a function of E_T for $Pb+Pb$ at 160 GeV. The experimental data are from Ref. [86], the histogram is a UrQMD calculation [87]. No scaling factor has been applied to the *x*-axis for either the calculations or the data.

the suppression. In fact, from three-fluid calculations, even with QGP phase included, only a moderate change of the average and local energy density with bombarding energy is predicted. This seems to strongly speak against drastic threshold effects in the charmonium production.

The strong dependence of these results on details, such as the treatment of the formation time or the time dependent dissociation cross section, remain to be studied further. Furthermore, quantum effects such as energy dependent formation and coherence lengths must be taken into account [91] before definite statements can be made with regard to the nature of the J/ψ suppression. Interpretations of the data based on plasma scenarios are also increasingly evolving away from the original Mott transition analog [92, 93].

Hence, the theoretical debate on the interpretation of the pattern of charmonium suppression discovered by NA38/NA50 at the SPS is far from settled. It is not clear whether the suppression is the smoking gun of non-equilibrium dynamics or deconfinement. It is not likely to be due to simple Debye screening.

The major goal of further theoretical work is not to continue to try to rule out more "conventional" explanations, but to give positive proof of additional suppression by QCD-calculations which actually *predict* the E_T-dependence of the conjectured signature. Consistency tests and a detailed simultaneous analysis of all other measured observables are needed, if at least the same standards as for the present calculations are to be hold up.

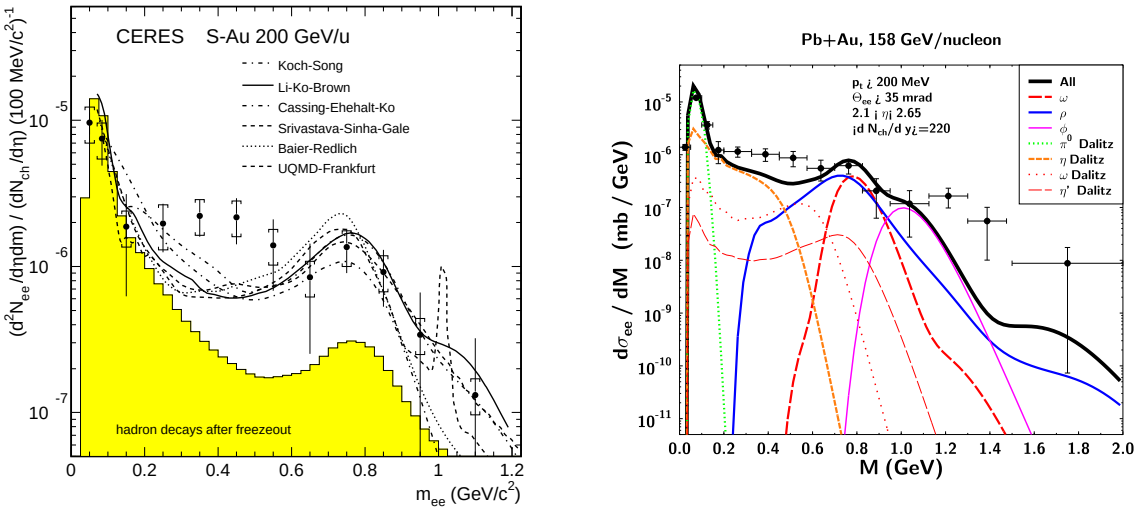

FIGURE 15. Left: inclusive e^+e^- mass spectra in 200 GeV/nucleon S+Au collisions as measured by the CERES collaboration [94]. The figures have been taken from [95]. The shaded area depicts hadronic contributions from resonance decays. The data are compared calculations based on a purely hadronic scenario [96, 97, 98, 99, 100]. Right: UrQMD prediction and data [101] for Pb+Au at 160 GeV/nucleon.

DILEPTON PRODUCTION

Beside results from hadronic probes, electromagnetic radiation – and in particular dileptons – offer an unique probe from the hot and dense reaction zone: here, hadronic matter is almost transparent.

Dileptons can carry information on the thermodynamic state of the medium at the moment of production. Since the dileptons interact only electromagnetically they can leave the hot and dense reaction zone basically undistorted.

The main background contributions stem from pion annihilation, resonance decays [102, 103, 104, 105, 106] (two pions can annihilate, forming either a virtual photon or a rho meson – both may then decay into a dilepton) and $\pi - \rho$ interactions [107, 108] at low dilepton masses and Drell–Yan processes [109, 110] at high masses . Furthermore meson resonances such as the rho-, omega- or phi- meson may be produced directly or in the decay of strings and heavier resonances. As all of those vector mesons carry the same quantum numbers as the photon, they may decay directly into a dilepton. Resonances can also emit dileptons via Dalitz decays. The Drell–Yan process describes the annihilation of a quark of one hadron with an anti-quark (in proton proton collisions from the sea of $\overline{q}$) of the other hadron, again resulting in a virtual photon which decays into a dilepton. The open charm contribution to the dilepton mass spectrum has been estimated to be negligible for low dilepton masses [111] at the CERN/SPS. At RHIC and LHC energies, however, charm contributions dominate the dilepton mass spectrum above 2 GeV [112].

Most original calculations on dileptons as signals of a QGP at CERN/SPS energies focused on masses below the rho meson mass [113, 114, 115, 116, 117, 103, 118, 119, 120, 121]. The current understanding of hadronic background contributions [102, 104, 105, 106] shows that most probably dileptons originating from a QGP are over-shined

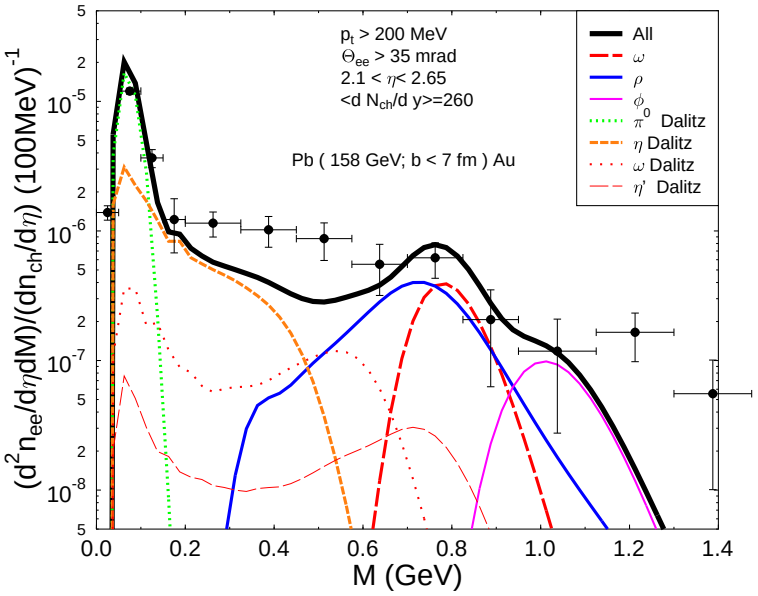

FIGURE 16. Microscopic calculation of the dilepton production in the kinematic acceptance region of the CERES detector for $Pb + Au$ collisions at 158 GeV. No in-medium effects are taken into account. Plotted data points are taken at CERES in '95.

by hadrons, with the possible exception of masses around 1 to 1.5 GeV [122, 123] where the rates from a plasma (at very high temperatures around 500 MeV) may suffice to be visible. At higher masses, the yield of Drell–Yan processes from first nucleon nucleon collisions most probably exceeds that of thermal dileptons from a QGP. Finite baryochemical potential will, at a given energy density, reduce the number of dileptons emitted from a QGP [124, 125, 126], due to the dropping temperature in that system.

The dependence of the yield of high mass dileptons on the thermalization time is still a point of open debate [127, 128]. The parton cascade [129] and other models of the early equilibration phase [128, 130] predict an excess of dileptons originating from an equilibrating QGP over the Drell–Yan background in the mass range between 5 and 10 GeV. Then the early thermal evolution of the deconfined phase could be traced in an almost model independent fashion [131].

The secondary dilepton production via quark-antiquark annihilation has also been studied on the basis of a hadronic transport code (UrQMD [2]). Here, one obtains a realistic collision spectrum of secondary hadrons for SPS energies. Using parton distribution functions and evaluating the contributions of all individual hadronic collisions one finds that meson-baryon interactions enhance the mass spectrum at mid-rapidity below masses of 3 GeV considerably [110]. Preresonance interactions are estimated to enhance this secondary yield by up to a factor of 5.

Dileptons can be measured at CERN in form of dimuons by the HELIOS3, NA38 and NA50 [132, 133, 134, 135] collaborations and in form of electron pairs by the CERES collaboration [94]. Dimuons exhibit an excess in AA collisions in the mass

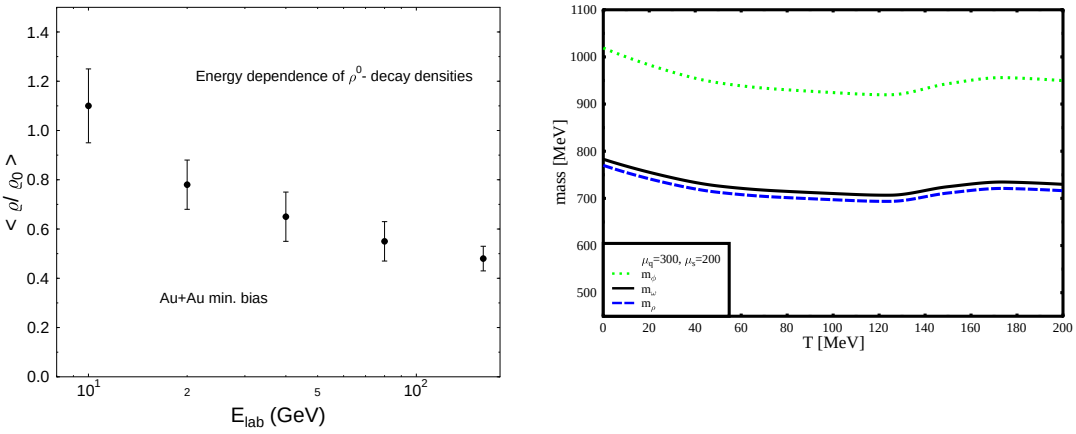

FIGURE 17. (Left) The mean "freeze-out" density at the location of ρ meson decays in $Au+Au$ collisions. (Right) The mass of the ρ-meson as obtained from the chiral model at different temperatures and finite density.

range $0.2 < M < 2.5$ GeV/c^2 up to the J/Ψ, as compared to pp and pA collisions. For dielectrons an excess is observed in the low–mass region $0.2 < M < 1.5$ GeV/c^2, again relative to pp and pA collisions (c.f. figure 15).

Both, the dielectron as well as the dimuon data seem to be compatible with a hydrodynamic approach assuming the creation of a thermalized QGP [97]. Hadronic transport calculations are not able to fully reproduce the observed excess [96, 136, 137]. However, at least part of the observed enhancement of lepton pairs at intermediate and low masses might be either caused by the previously neglected source of secondary Drell-Yan processes [110] or by contributions of heavy mesons, such as the a_1 [138].

The observed enhancement of the dilepton yield at intermediate invariant masses ($M_{e^+e^-} > 0.3$ GeV) received great interest: it was prematurely thought that the lowering of vector meson masses is required by chiral symmetry restoration (see e.g. [139] for a review). However, there seems no theoretical support for this speculation. Calculations within a chiral $SU(3)$ mean-field approach [47] show only a modest dependence of temperature of the mass of the ρ meson (Fig. 17, right). AA-data are compatible with broadening spectral functions found in pure hadronic calculations of the scattering on the constituents of the excited matter (see e.g. [140]). The present data do not allow to draw definite conclusions.

Fig. 16 shows a microscopic UrQMD calculation of the dilepton production in the kinematic acceptance region of the CERES detector for $Pb+Au$ collisions at 158 GeV. This is compared with the '95 CERES data [101]. Aside from the difference at $M \approx 0.4$ GeV there is a strong enhancement at higher invariant masses. It is expected that this discrepancy at $m > 1$ GeV could be filled up by direct dilepton production in meson-meson collisions [141] as well as by the mechanism of secondary Drell-Yan pair production proposed in [110].

The mean "freeze-out" density at the location of ρ meson decays in $Au+Au$ collisions

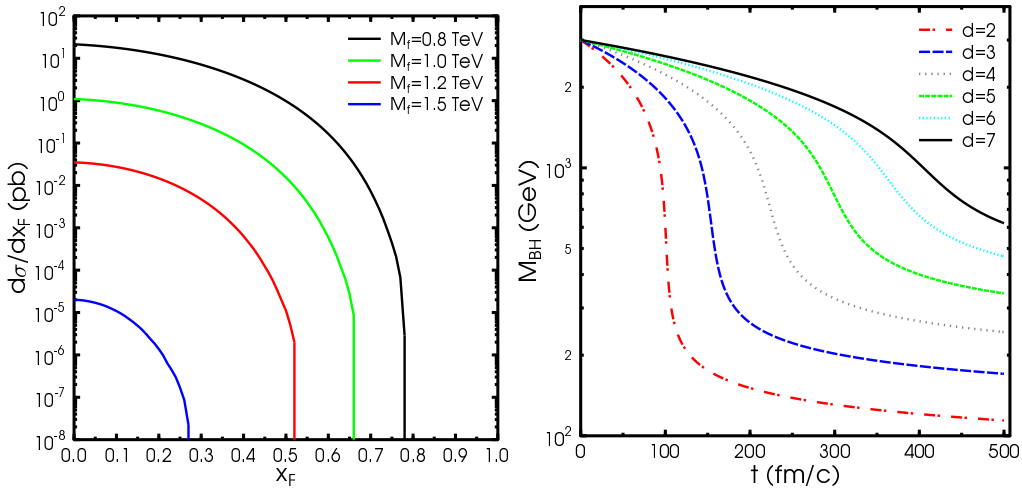

FIGURE 18. (Left:) The Feynman-x distribution of black holes for $M \geq M_f$ TeV in proton-proton interactions. (Right:) Time evolution of the mass of evaporating black holes produced at LHC. Different lines correspond to different numbers of extra dimensions d [143].

is shown in Fig. 17 (left) for different incident energies [142]. From AGS to CERN energies, there is a decrease of the baryonic density, indicating that baryonic modifications to the ρ meson are better studied at energies of $20-40$ AGeV. The low baryon densities at high energies will make it hard to explain the CERES data by ρ meson modifications of nucleonic origin alone.

CREATION OF BLACK HOLES IN LARGE HADRON COLLIDER

An exciting new idea, marking the end of short distance physics as we know it from perturbative QCD, may be the production of black holes at energies reached in collisions at the LHC.

This thrilling possibility is a consequence of reasoning about the existence of extra dimensions beyond the usual, well-known 4 space-time dimensions. These ideas have been motivated by string theories, and they offer a unique opportunity to tackle the so called hierarchy problem, the large gap between the electroweak energy scale ($m_{\rm W} = 10^3$ GeV) and the Planck scale as we know it ($m_{\rm Planck} = 10^{19}$ GeV).

In scenarios with d compact, so called large extra-dimension (LXD, "large" means here scales up to millimeter – in contrast to the tiny compactification radii in usual string or Kaluza-Klein theories in the order of the Planck length), the fundamental energy scale $m_{\rm f}$ might be as big as $m_{\rm W}$, reaching the TeV region [144, 145, 146]. But since only gravity would propagate in the extra dimensions, while the fields and particles of the standard model would be constrained to the well known 4 space-time dimensions, this would allow the large value of our 4-dimensional Planck mass $m_{\rm Planck}$.

The possibility that the fundamental energy scale, $m_{\rm f}$, might be as low as the electroweak scale $m_{\rm W}$ makes the future high energy colliders CLIC, LHC and TESLA capable of producing black holes. A black hole would be produced whenever the energy

of the collision were concentrated in a region of space small enough to be trapped inside the Schwarzschild horizon corresponding to the energy involved. However, due to Hawking radiation, the black hole decays again, spitting out all kinds of standard model particles. The problem is to find signatures of the creation and subsequent evaporation of the black hole.

For non-spinning black holes, figure 18 depicts the momentum distribution of black holes produced in pp collisions[147]. Many of the black holes are formed in scattering processes of valence quarks. The dependence of the cross section on the number of extra dimensions is less than 10%.

The time evolution of the black hole can be seen in Figure 18 for different numbers of compactified space-like extra dimensions. Extra dimensions lead to an increase in the lifetime of the black hole. It can be seen from the calculations depicted in figure 18 that for $d = 2$, a black hole with mass $\sim$ TeV exists for at least 100 fm/c [148]. Afterwards the mass drops below the fundamental scale.

The effects of LXDs allow for the creation of 10^7 black holes with lifetime τ=(10-600)fm/c per year at LHC. Hawking radiation is also suppressed with large extra dimensions. The prediction of the suppression of jets with high p_T due to the formation of black holes in the final state will be a clear signature for extra dimensions. Maybe with LHC particle physicists will be able to compete with astronomers in the field of observing black holes.

OUTLOOK

At the CERN/SPS new data on flow, electro-magnetic probes, strange particle yields (most importantly multi-strange (anti-)hyperons) and heavy quarkonia are interesting to follow closely. Simple energy densities estimated from rapidity distributions and temperatures extracted from particle spectra indicate that initial conditions could be near or just above the domain of deconfinement and chiral symmetry restoration. Still the quest for an *unambiguous* signature remains open.

Directed flow has been discovered – now a flow excitation function, filling the gap between 10 AGeV (AGS) and 160 AGeV (SPS), would be extremely interesting: look for the softening of the QCD equation of state in the coexistence region. The investigation of the physics of high baryon density (e.g. partial restoration of chiral symmetry via properties of vector mesons) is presently not accessible due to the lack of dedicated accelerators in the $10-200$ AGeV regime. The achieved and planned 40 AGeV and 80 AGeV runs at CERN are an absolute necessity into this new direction, but it can only be a first step.

However, dedicated accelerators would be mandatory to explore these intriguing effects in the excitation function. It is questionable whether this key program will actually get support at CERN. In this respect, the planned new machine at GSI, SIS/200, will be of extreme importance. Also the excitation function of particle yield ratios ($\pi/\mathrm{p}, \mathrm{d}/\mathrm{p}, \mathrm{K}/\pi$...) and, in particular, multi-strange (anti-)hyperon yields, can be a sensitive probe of physics changes in the EoS. The search for novel, unexpected forms of $SU(3)$ matter, e.g. *hypermatter*, *strangelets* or even *charmlets* is intriguing. Such ex-

otic QCD multi-meson and multi-baryon configurations would extend the present periodic table of elements into hitherto unexplored dimensions. A strong experimental effort should continue in that direction.

Experiments and data on ultra-relativistic collisions are essential in order to motivate, guide, and constrain theoretical developments. They provide the only terrestrial probes of non-perturbative aspects of QCD and its dynamical vacuum. The understanding of confinement and chiral symmetry – and the possibility of even gaining glimpses of the realm of quantum gravity – remains one of the key questions at the beginning of this millennium.

ACKNOWLEDGMENTS

This work was supported by DFG, GSI, BMBF, Graduiertenkolleg Theoretische und Experimentelle Schwerionenphysik, the A. v. Humboldt Foundation, and the J. Buchmann Foundation.

REFERENCES

1. Brachmann, J., Dumitru, A., Maruhn, J. A., Stocker, H., Greiner, W., and Rischke, D. H., *Nucl. Phys.*, **A619**, 391–412 (1997).
2. Bass, S. A., Belkacem, M., Bleicher, M., Brandstetter, M., Bravina, L., Ernst, C., Gerland, L., Hofmann, M., Hofmann, S., Konopka, J., Mao, G., Neise, L., Soff, S., Spieles, C., Weber, H., Winckelmann, L. A., Stocker, H., Greiner, W., Hartnack, C., Aichelin, J., and Amelin, N., *Prog. Part. Nucl. Phys.*, **41**, 225–370 (1998).
3. Rosenhauer, A., Csernai, L. P., Maruhn, J. A., and Greiner, W., *Phys. Scripta*, **30**, 45–51 (1984).
4. Geiger, K., *Nucl. Phys.*, **A638**, 551c–554c (1998).
5. Weber, H., et al., *to be publ.* (2002).
6. Hofmann, M., Bleicher, M., Scherer, S., Neise, L., Stocker, H., and Greiner, W., *Phys. Lett.*, **B478**, 161–171 (2000).
7. Scherer, S., Hofmann, M., Bleicher, M., Neise, L., Stocker, H., and Greiner, W., *New Jour. Phys.*, **3**, 8 (2001).
8. Scheid, W., Ligensa, R., and Greiner, W., *Phys. Rev. Lett.*, **21**, 1479–1482 (1968).
9. Chapline, G. F., Johnson, M. H., Teller, E., and Weiss, M. S., *Phys. Rev.*, **D8**, 4302–4308 (1973).
10. Scheid, W., Muller, H., and Greiner, W., *Phys. Rev. Lett.*, **32**, 741–745 (1974).
11. Boguta, J., *Phys. Lett.*, **B109**, 251 (1981).
12. Li, Z.-X., Mao, G.-J., Zhuo, Y.-Z., and Greiner, W., *Phys. Rev.*, **C56**, 1570–1575 (1997).
13. Bjorken, J. D., *Phys. Rev.*, **D27**, 140–151 (1983).
14. Hartnack, C., Zhuxia, L., Neise, L., Peilert, G., Rosenhauer, A., Sorge, H., Aichelin, J., Stocker, H., and Greiner, W., *Nucl. Phys.*, **A495**, 303c–320c (1989).
15. Berenguer, M., et al., *J. Phys.*, **G18**, 655–679 (1992).
16. Schmidt, W., Katscher, U., Waldhauser, B., A. Maruhn, J., Stocker, H., and Greiner, W., *Phys. Rev.*, **C47**, 2782–2793 (1993).
17. Gyulassy, M., and Greiner, W., *Annals Phys.*, **109**, 485–527 (1977).
18. Harris, J. W., and Muller, B., *Ann. Rev. Nucl. Part. Sci.*, **46**, 71–107 (1996).
19. Blobel, V., et al., *Nucl. Phys.*, **B69**, 454–492 (1974).
20. Abbott, T., et al., *Phys. Rev.*, **C50**, 1024–1047 (1994).
21. Barrette, J., et al., *Phys. Rev.*, **C50**, 3047–3059 (1994).
22. Baechler, J., et al., *Phys. Rev. Lett.*, **72**, 1419–1422 (1994).
23. Stocker, H., and Greiner, W., *Phys. Rept.*, **137**, 277–392 (1986).

24. Clare, R. B., and Strottman, D., *Phys. Rept.*, **141**, 177–280 (1986).
25. Hofmann, M., Mattiello, R., Sorge, H., Stocker, H., and Greiner, W., *Phys. Rev.*, **C51**, 2095–2098 (1995).
26. Sorge, H., Keitz, A. v., Mattiello, R., Stocker, H., and Greiner, W., *Phys. Lett.*, **B243**, 7 (1990).
27. von Keitz, A., Winckelmann, L., Jahns, A., Sorge, H., Stocker, H., and Greiner, W., *Phys. Lett.*, **B263**, 353–358 (1991).
28. Sorge, H., Berenguer, M., Stocker, H., and Greiner, W., *Phys. Lett.*, **B289**, 6–11 (1992).
29. Pang, Y., Schlagel, T. J., and Kahana, S. H., *Phys. Rev. Lett.*, **68**, 2743–2746 (1992).
30. Aichelin, J., and Werner, K., *Phys. Lett.*, **B300**, 158–162 (1993).
31. Rischke, D. H., Pursun, Y., Maruhn, J. A., Stocker, H., and Greiner, W., *Heavy Ion Phys.*, **1**, 309 (1995).
32. Hofmann, J., Stocker, H., Heinz, U. W., Scheid, W., and Greiner, W., *Phys. Rev. Lett.*, **36**, 88–91 (1976).
33. Hartnack, C., Stocker, H., and Greiner, W., in *Proceedings of the Nato Advanced Study Institute on the Nuclear Equation of State*, Plenum Press, 1990.
34. Brachmann, J., et al., *Phys. Rev.*, **C61**, 024909 (2000).
35. Sorge, H., von Keitz, A., Mattiello, R., Stoecker, H., and Greiner, W., *Phys. Lett.*, **B243**, 7–12 (1990).
36. Fermi, E., *Prog. Theor. Phys.*, **5**, 570–583 (1950).
37. Landau, L. D., *Izv. Akad. Nauk SSSR Ser. Fiz.*, **17**, 51–64 (1953).
38. Hahn, D., and Stocker, H., *Nucl. Phys.*, **A452**, 723–737 (1986).
39. Braun-Munzinger, P., Heppe, I., and Stachel, J., *Phys. Lett.*, **B465**, 15–20 (1999).
40. Rafelski, J., and Letessier, J., *nucl-th/9903018* (1999).
41. Becattini, F., Cleymans, J., Keranen, A., Suhonen, E., and Redlich, K., *Phys. Rev.*, **C64**, 024901 (2001).
42. Yen, G. D., and Gorenstein, M. I., *Phys. Rev.*, **C59**, 2788–2791 (1999).
43. Braun-Munzinger, P., Magestro, D., Redlich, K., and Stachel, J., *Phys. Lett.*, **B518**, 41–46 (2001).
44. Braun-Munzinger, P., and Stachel, J., *Nucl. Phys.*, **A638**, 3–18 (1998).
45. Siemens, P. J., and Kapusta, J. I., *Phys. Rev. Lett.*, **43**, 1486–1489 (1979).
46. Gorenstein, M. I., Rischke, D. H., Stocker, H., Greiner, W., and Bugaev, K. A., *J. Phys.*, **G19**, L69–L75 (1993).
47. Papazoglou, P., Zschiesche, D., Schramm, S., Schaffner-Bielich, J., Stocker, H., and Greiner, W., *Phys. Rev.*, **C59**, 411–427 (1999).
48. Zschiesche, D., P. Papazoglou, P., Schramm, S., Beckmann, C., Schaffner-Bielich, J., Stocker, H., and Greiner, W., *Springer Tracts Mod. Phys.*, **163**, 129 (2000).
49. Zschiesche, D., Schramm, S., Stocker, H., and Greiner, W., *Phys. Rev.*, **C65**, 064902 (2002).
50. Michalec, M., *nucl-th/0112044* (2001).
51. Zschiesche, D., et al., *to be publ.* (2002).
52. Michalec, M., Florkowski, W., and Broniowski, W., *Phys. Lett.*, **B520**, 213–216 (2001).
53. Bass, S. A., Belkacem, M., Brandstetter, M., Bleicher, M., Gerland, L., Konopka, J., Neise, L., Spieles, C., Soff, S., Weber, H., Stocker, H., and Greiner, W., *Phys. Rev. Lett.*, **81**, 4092–4095 (1998).
54. Bravina, L. V., I. Gorenstein, M. I., Belkacem, M., Bass, S. A., Bleicher, M., Brandstetter, M., Hofmann, M., Soff, S., Spieles, C., Weber, H., Stocker, H., and Greiner, W., *Phys. Lett.*, **B434**, 379–387 (1998).
55. Reiter, M., Dumitru, A., Brachmann, J., Maruhn, J. A., Stocker, H., and W., G., *Nucl. Phys.*, **A643**, 99–112 (1998).
56. Braun-Munzinger, P., Stachel, J., Wessels, J. P., and Xu, N., *Phys. Lett.*, **B344**, 43–48 (1995).
57. Wong, C.-Y., *Introduction to High-Energy Heavy-Ion Collisions*, World Scientific, 1994.
58. Andersen, E., et al., *Phys. Lett.*, **B433**, 209–216 (1998).
59. Ivanenko, D. D., and Kurdgelaidze, D. F., *Astrophys.*, **1**, 251 (1965).
60. Bodmer, A. R., *Phys. Rev.*, **D4**, 1601–1606 (1971).
61. Chin, S. A., and Kerman, A. K., *Phys. Rev. Lett.*, **43**, 1292 (1979).
62. Farhi, E., and Jaffe, R. L., *Phys. Rev.*, **D30**, 2379 (1984).
63. Witten, E., *Phys. Rev.*, **D30**, 272–285 (1984).

64. Chodos, A., Jaffe, R. L., Johnson, K., Thorn, C. B., and Weisskopf, V. F., *Phys. Rev.*, **D9**, 3471–3495 (1974).
65. Michel, F. C., *Phys. Rev. Lett.*, **60**, 677–679 (1988).
66. Greiner, C., Koch, P., and Stocker, H., *Phys. Rev. Lett.*, **58**, 1825–1828 (1987).
67. Lukacs, B., Zimanyi, J., and Balazs, N. L., *Phys. Lett.*, **B183**, 27 (1987).
68. Schaffner-Bielich, J., Greiner, C., Diener, A., and Stocker, H., *Phys. Rev.*, **C55**, 3038–3046 (1997).
69. Schaffner, J., Stocker, H., and Greiner, C., *Phys. Rev.*, **C46**, 322–329 (1992).
70. Prowse, D. J., *Phys. Rev. Lett.*, **17**, 782–785 (1966).
71. Baltz, A. J., et al., *Phys. Lett.*, **B325**, 7–12 (1994).
72. Shiva Kumar, B., *Nucl. Phys.*, **A590**, 29c–45c (1995).
73. Rotondo, F. S., et al., *Nucl. Phys.*, **A610**, 297c–305c (1996).
74. Barish, K. N., *Heavy Ion Phys.*, **4**, 423–428 (1996).
75. Borer, K., et al., *Phys. Rev. Lett.*, **72**, 1415–1418 (1994).
76. Dittus, F., et al., *Nucl. Phys.*, **A590**, 347c–354c (1995).
77. Klingenberg, R., et al., *Nucl. Phys.*, **A610**, 306c–316c (1996).
78. Appelquist, G., et al., *Phys. Rev. Lett.*, **76**, 3907–3910 (1996).
79. Beringer, J., et al., "Search for strangelets and production of antinuclei in Pb+Pb collisions at CERN," in *Structure of Vacuum and Elementary Matter*, edited by H. Stocker, A. Gallmann, and J. Hamilton, 1996, international Conference on Nuclear Physics at the Turn of Millennium, Wilderness / George, South Africa.
80. Ambrosini, G., et al., *Nucl. Phys.*, **A638**, 411–414 (1998).
81. Harris, J. W., *Nucl. Phys.*, **A566**, 277c–285c (1994).
82. Schukraft, J., "Little bang at big colliders: Heavy ion physics at LHC and RHIC," in *Structure of Vacuum and Elementary Matter*, edited by H. Stocker, A. Gallmann, and J. Hamilton, 1996, international Conference on Nuclear Physics at the Turn of Millennium, Wilderness / George, South Africa.
83. Spieles, C., et al., *Phys. Rev. Lett.*, **76**, 1776–1779 (1996).
84. Matsui, T., and Satz, H., *Phys. Lett.*, **B178**, 416 (1986).
85. Gerland, L., Frankfurt, L., Strikman, M., Stocker, H., and Greiner, W., *Phys. Rev. Lett.*, **81**, 762–765 (1998).
86. Romana, A., "Anomalous J/ψ suppression in Pb+Pb collisions," in *Proceedings of XXXIIIrd Rencontres de Moriond*, 1998.
87. Spieles, C., Vogt, R., Gerland, L., Bass, S. A., Bleicher, M., Frankfurt, L., Strikman, M., Stocker, H., and Greiner, W., *Phys. Rev.*, **C60**, 054901 (1999).
88. Neubauer, D., Sailer, K., Muller, B., Stocker, H., and Greiner, W., *Mod. Phys. Lett.*, **A4**, 1627 (1989).
89. Gavin, S., and Vogt, R., *Nucl. Phys.*, **B345**, 104–124 (1990).
90. Gavin, S., and Vogt, R., *Phys. Rev. Lett.*, **78**, 1006–1009 (1997).
91. Hufner, J., and Kopeliovich, B., *nucl-th/9606010* (1996).
92. Kharzeev, D., Lourenco, C., Nardi, M., and Satz, H., *Z. Phys.*, **C74**, 307–318 (1997).
93. Satz, H., *Nucl. Phys.*, **A642**, 130–142 (1998).
94. Agakishiev, G., et al., *Phys. Rev. Lett.*, **75**, 1272–1275 (1995).
95. Drees, A., *Nucl. Phys.*, **A610**, 536c–551c (1996).
96. Winckelmann, L. A., et al., *Nucl. Phys.*, **A610**, 116c–123c (1996).
97. Srivastava, D. K., Sinha, B., Pal, D., Gale, C., and Haglin, K., *Nucl. Phys.*, **A610**, 350c–357c (1996).
98. Cassing, W., Ehehalt, W., and Ko, C. M., *Phys. Lett.*, **B363**, 35–40 (1995).
99. Li, G.-Q., Ko, C. M., and Brown, G. E., *Phys. Rev. Lett.*, **75**, 4007–4010 (1995).
100. Koch, V., and Song, C., *Phys. Rev.*, **C54**, 1903–1917 (1996).
101. Agakishiev, G., et al., *Phys. Lett.*, **B422**, 405–412 (1998).
102. Cleymans, J., Redlich, K., and Satz, H., *Z. Phys.*, **C52**, 517–526 (1991).
103. Koch, P., *Z. Phys.*, **C57**, 283–304 (1993).
104. Gale, C., and Lichard, P., *Phys. Rev.*, **D49**, 3338–3344 (1994).
105. Song, C., and Ko, C., C. M.and Gale, *Phys. Rev.*, **D50**, R1827–R1831 (1994).
106. Winckelmann, L. A., Sorge, H., Stocker, H., and Greiner, W., *Phys. Rev.*, **C51**, 9–11 (1995).
107. Baier, R., Dirks, M., and Redlich, K., *Phys. Rev.*, **D55**, 4344–4354 (1997).
108. Murray, J., Bauer, W., and Haglin, K., *Phys. Rev.*, **C57**, 882–888 (1998).

109. Drell, S. D., and Yan, T.-M., *Phys. Rev. Lett.*, **25**, 316–320 (1970).
110. Spieles, C., Gerland, L., Hammon, N., Bleicher, M., Bass, S. A., Stoecker, H., Greiner, W., Lourenco, C., and Vogt, R., *Eur. Phys. J.*, **C5**, 349–355 (1998).
111. Braun-Munzinger, P., Miskowiec, D., Drees, A., and Lourenco, C., *Eur. Phys. J.*, **C1**, 123–130 (1998).
112. Gavin, S., McGaughey, P. L., Ruuskanen, P. V., and Vogt, R., *Phys. Rev.*, **C54**, 2606–2623 (1996).
113. Shuryak, E. V., *Phys. Lett.*, **B78**, 150 (1978).
114. Domokos, G., and Goldman, J. I., *Phys. Rev.*, **D23**, 203 (1981).
115. Kajantie, K., and Miettinen, H. I., *Zeit. Phys.*, **C9**, 341 (1981).
116. Kajantie, K., and Miettinen, H. I., *Z. Phys.*, **C14**, 357–362 (1982).
117. Chin, S. A., *Phys. Lett.*, **B119**, 51–56 (1982).
118. Cleymans, J., and Fingberg, J., *Phys. Lett.*, **B168**, 405 (1986).
119. Cleymans, J., Fingberg, J., and Redlich, K., *Phys. Rev.*, **D35**, 2153 (1987).
120. Siemens, P. J., and Chin, S. A., *Phys. Rev. Lett.*, **55**, 1266–1268 (1985).
121. Seibert, D., *Phys. Rev. Lett.*, **68**, 1476–1479 (1992).
122. Ruuskanen, P. V., *Nucl. Phys.*, **A525**, 255–268 (1991).
123. Ruuskanen, P. V., *Nucl. Phys.*, **A544**, 169–182 (1992).
124. Ko, C. M., and Xia, L. H., *Phys. Rev. Lett.*, **62**, 1595–1598 (1989).
125. Dumitru, A., et al., *Phys. Rev. Lett.*, **70**, 2860–2863 (1993).
126. He, Z.-J., and Zhang, J.-J., *J. Phys.*, **G21**, L49–L55 (1995).
127. Kapusta, J., McLerran, L. D., and Kumar Srivastava, D., *Phys. Lett.*, **B283**, 145–150 (1992).
128. Kampfer, B., and Pavlenko, O. P., *Phys. Lett.*, **B289**, 127–131 (1992).
129. Geiger, K., and Kapusta, J. I., *Phys. Rev. Lett.*, **70**, 1920–1923 (1993).
130. Shuryak, E. V., and Xiong, L., *Phys. Rev. Lett.*, **70**, 2241–2244 (1993).
131. Strickland, M., *Phys. Lett.*, **B331**, 245–250 (1994).
132. Mazzoni, M. A., *Nucl. Phys.*, **A566**, 95c–102c (1994).
133. Masera, M., *Nucl. Phys.*, **A590**, 93c–102c (1995).
134. Lourenco, C., et al., *Nucl. Phys.*, **A566**, 77c–85c (1994).
135. Gonin, M., et al., *Nucl. Phys.*, **A610**, 404c–417c (1996).
136. Ko, C. M., Li, G.-Q., Brown, G. E., and Sorge, H., *Nucl. Phys.*, **A610**, 342c–349c (1996).
137. Bratkovskaya, E. L., and Cassing, W., *Nucl. Phys.*, **A619**, 413–446 (1997).
138. Li, G.-Q., Brown, G. E., Gale, C., and Ko, C. M., *nucl-th/9712048* (1997).
139. Koch, V., *Int. J. Mod. Phys.*, **E6**, 203–250 (1997).
140. Cassing, W., Bratkovskaya, E. L., Rapp, R., and Wambach, J., *Phys. Rev.*, **C57**, 916–921 (1998).
141. Li, G.-Q., and Gale, C., *Phys. Rev.*, **C58**, 2914–2927 (1998).
142. Winckelmann, L. A., *Ultrarelativistische Quanten-Molekular-Dynamik: Ein Modell zur Simulation von Schwerionen-Reaktionen*, Ph.D. thesis, Johann Wolfgang Goethe Universität (1996).
143. Hossenfelder, S., Hofmann, S., Bleicher, M., and Stocker, H., *hep-ph/0109085* (2001).
144. Arkani-Hamed, N., Dimopoulos, S., and Dvali, G. R., *Phys. Lett.*, **B429**, 263–272 (1998).
145. Arkani-Hamed, N., Dimopoulos, S., and Dvali, G. R., *Phys. Rev.*, **D59**, 086004 (1999).
146. Antoniadis, I., Arkani-Hamed, N., Dimopoulos, S., and Dvali, G. R., *Phys. Lett.*, **B436**, 257–263 (1998).
147. Bleicher, M., Hofmann, S., Hossenfelder, S., and Stocker, H., *hep-ph/0112186* (2001).
148. Hofmann, S., et al., *hep-ph/0111052* (2001).